J. KSIAM Vol.10, No.1, 35-54, 2006

ACCURATE AND EFFICIENT RE-EVALUATION OF CELL-INTERFACE CONVECTIVE FLUXES

Kyung-Lok Lee, Sung-Hwan Yoon, Chongam Kim and Kyu-Hong Kim

ABSTRACT In order to reduce the excessive numerical dissipation which is induced when a grid system is not aligned with a discontinuity, a new spatial treatment of cell-interface fluxes is introduced. The M-AUSMPW+ in this paper has the formula that has an additional procedure of re-defining transferred properties at a cell-interface, based on AUSMPW+. The newly defined transferred property could eliminate numerical dissipation effectively in non-flow aligned grid system of multi-dimensional flows. Through several test cases M-AUSMPW+ proves to be efficient and about twice more accurate than conventional upwind schemes. The three-dimensional implementation of M-AUSMPW+ is expected to provide accuracy and efficiency improvement furthermore.

1. INTRODUCTION

Up to now, most popular numerical schemes have been developed based on one-dimensional flow physics. However, due to the essential limitations of this approach in the accurate and efficient calculations of three-dimensional flows, multi-dimensional flow physics needs to be incorporated as much as possible at the design stage of numerical flux functions. In discretizing the governing equations of fluid motions, some degree of numerical errors is inevitably introduced. With the help of many previous studies, a numerical scheme at present can remove errors almost completely in one-dimensional contact or shock discontinuity. It means that the present CFD technique can give very satisfactory results in one-dimensional problems. However, when applied to two- or three- dimensional flows, numerical scheme frequently generates large errors and accuracy becomes deteriorated. In case of three-dimensional computations, it is especially conspicuous. Thus, a denser grid system is necessary, and as a consequence, a large amount of data storage and computational cost are entailed.

In analyzing those complex phenomena, accurate and efficient numerical methods reflecting multi-dimensional flow physics are critical. we describe new numerical approaches which give much better results in multi-dimensional problems. The main focus is to develop numerical methods that eliminate excessive numerical dissipation and upgrade solution accuracy by predicting the physical distribution of flow variables more accurately in multi-space dimensions.

A spatial discretization technique is newly developed based on AUSM-type scheme [1]. The core

AMS Subject Classification:
Key Words and Phrases: Multi-dimensional flow computations, Advection property, AUSM-type method, M-AUSMPW+, TVD limiting condition, MUSCL

idea of the new scheme is to modify the convective quantity at a cell-interface by reflecting physical and multi-dimensional phenomena. In case of the present method, a criterion to predict more accurate cell-interface state is proposed through the analysis of TVD limiters [3, 4, 5], and the convective quantity at a cell-interface is *re-evaluated* according to the criterion. The advantages of the newly determined convective quantity can be examined in two aspects. Firstly, it provides the closer cell-interface approximation of the real physical value than previous approaches. Secondly, it can eliminate numerical dissipation effectively in a non-aligned grid system. As a result, the present method can improve solution accuracy significantly, especially, in smooth region including contact or slip discontinuity. From extensive numerical analyses and calculations, it is observed that the present method is very useful in multi-dimensional flow computations without compromising computational cost. For that reason, it is coined M-AUSMPW+ which represents AUSMPW+ scheme for Multi-dimensional flow calculations.

2. KEY IDEAS AND IMPROVEMENTS OF BASELINE SCHEME

2.1. Re-evaluation of cell-interface fluxes

The advantage of upwind scheme is that it can represent flow physics properly through the whole Mach number range, *i.e.*, it transfers flow information correctly according to the local feature of wave physics. As a result, upwind scheme can capture discontinuity accurately and robustly. Aside from this, numerical dissipation can be automatically determined through the whole Mach number range. Thus, it is less dependent on user experience. In spite of such merits, upwind scheme seems to provide excessive numerical dissipation in continuous region because it is designed to have optimal numerical dissipation in discontinuity, *i.e.*, it looks more appropriate in discontinuous region.

Therefore, if an upwind scheme contains extra step to distinguish continuous region from discontinuous region, or gently varied region from rapidly varied region, it can provide low dissipative/more accurate results. With regard to this issue, the first objective of the present paper is to introduce a procedure to differentiate continuous region from discontinuous region. The second objective is to improve the shock capturing capability of AUSMPW+ to yield monotonic profile in a steady flow. Even though AUSMPW+ has been developed to remove the overshoot problem of AUSM-type schemes, it is still not perfect since it shows a little overshoot under some condition (see Fig.5.) and convergence becomes bad in some grid system [1]. Monotonic shock capturing property reduces grid dependency and improves convergence in all grid systems.

AUSM-type schemes define the Mach number at a cell-interface and transfer the flux quantity according to its sign, which is called the advection property. The convective flux of AUSM-type schemes is written as follows.

$$\mathbf{F}_{\frac{1}{2}} = m_{\frac{1}{2}} c_{\frac{1}{2}} \Psi_{L \text{ or } R}, \tag{1}$$

where $m_{1/2}$ is the cell-interface Mach number and Ψ is the transferred quantity vector. If a flux function can recognize the difference between the region of discontinuity and continuity more clearly, it can give more accurate results. As a flexible way to clarify the two regions, the following flux form is considered.

$$\mathbf{F}_{\frac{1}{2}} = m_{\frac{1}{2}} c_{\frac{1}{2}} \Psi_{L \text{ or } R, \frac{1}{2}}, \tag{2}$$

where the subscript $\frac{1}{2}$ represents the quantity defined at a cell-interface. Simply stated, the fundamental difference from previous AUSM-type schemes is to modify the convective quantity at a cell-interface appropriately in discontinuous and continuous regions. The convective quantity, $\Psi_{L,R,\frac{1}{2}}$, is determined to satisfy the following requirements.

r1. In order to increase accuracy in continuous region, the convective quantity should be able to distinguish the region of continuity from discontinuity, or expressing it more mildly, gently varied region from rapidly varied region.
r2. The convective quantity should satisfy the monotonic condition.
r3. The convective quantity should maintain the upwind characteristic in supersonic flow.

Requirement 1 is the major objective of the present paper. Requirement 2 is necessary to prevent oscillatory behaviors across discontinuities. The final requirement is essential to represent physical phenomena correctly in supersonic flow.

Requirement 1:

Since the transferred quantity vector $\Psi=(\rho,\rho u,\rho H)^T$ is calculated by primitive variable vector $\Phi=(\rho,u,p)^T$, re-evaluating procedure is explained using primitive variable vector.

Firstly, the characteristics of continuous and discontinuous regions are examined to establish the criterion that divides the two regions. The convective quantity at a cell-interface is then re-evaluated according to the criterion. The ideal case would be that the Mach number and convective quantity at a cell-interface are exactly the same as the physical values. Alternatively, if we can find out $\Phi_{L,R,\frac{1}{2}}$ which is closer to the real physical value than $\Phi_{L\,or\,R}$, Eq.(2) will be very effective.

In order to obtain information on the distribution of the physical value, TVD interpolation [3, 4] is analyzed. All the vector notations are introduced for compact expression. Thus, in actual implementation, they should be applied component by component. Through interpolation step, cell-interface quantities are prepared as

$$\Phi_L=\overline{\Phi}_i+0.5\Delta\Phi\big|_i=\overline{\Phi}_i+0.5\phi(r_L)\Delta\Phi_{i-\frac{1}{2}}, \tag{3a}$$

$$\Phi_R=\overline{\Phi}_{i+1}-0.5\Delta\Phi\big|_{i+1}=\overline{\Phi}_{i+1}-0.5\phi(r_R)\Delta\Phi_{i+\frac{3}{2}}, \tag{3b}$$

where Φ is TVD limiter and $r_L=\frac{\Delta\Phi_{i+\frac{1}{2}}}{\Delta\Phi_{i-\frac{1}{2}}}$, $r_R=\frac{\Delta\Phi_{i+\frac{3}{2}}}{\Delta\Phi_{i+\frac{1}{2}}}$. And variation at each cell-interface is defined as follows.

$$\Delta\Phi_{i-\frac{1}{2}}=\overline{\Phi}_i-\overline{\Phi}_{i-1},\quad \Delta\Phi_{i+\frac{1}{2}}=\overline{\Phi}_{i+1}-\overline{\Phi}_i,\quad \Delta\Phi_{i+\frac{3}{2}}=\overline{\Phi}_{i+2}-\overline{\Phi}_{i+1} \tag{4}$$

where the bar means a cell averaged value.

Except for the region of local extrema, the accuracy of TVD interpolation (Eqs.(4)) can be expressed by Taylor expansion with respect to the location of $i+\frac{1}{2}$ as

$$\Phi_{L,R}=\Phi_{i+\frac{1}{2}}+\Delta x^2\Phi''\left[\frac{1}{2}\phi'(1)-\frac{1}{3}\right]+O(\Delta x^3), \tag{5a}$$

$$\Phi_{L,R,\frac{1}{2}}=0.5(\Phi_L+\Phi_R)=\Phi_{i+\frac{1}{2}}+\frac{\Delta x^2}{2}\Phi''\left[\left(\frac{1}{2}\phi(1)-\frac{1}{3}\right)_L+\left(\frac{1}{2}\phi(1)-\frac{1}{3}\right)_R\right]+O(\Delta x^3). \tag{5b}$$

The leading error term is second order and becomes third order accurate if $\phi'(1)=2/3$. Let us consider the case that physical property is represented as Φ_{real} and it satisfies the concave condition of $\partial\Phi_{real}/\partial x>0$ and $\partial^2\Phi_{real}/\partial x^2>0$ as in Fig.1, where $r_L>1$ and $0<r_R<1/r_L$.

At first, minmod limiter is considered as the most diffusive second order TVD interpolation. It chooses the smallest variation of the two candidates as

$$\phi(r)=\max(0,\min(r,1)). \tag{6}$$

When $r_L>1$ and $0<r_R<1/r_L$, it gives

$$\Phi_{L,\min\,\mathrm{mod}}=\Phi_{real,i+\frac{1}{2}}-\frac{\Delta x^2}{3}\Phi''+O(\Delta x^3), \tag{7a}$$

$$\Phi_{R,\min\,\mathrm{mod}}=\Phi_{real,i+\frac{1}{2}}+\frac{\Delta x^2}{6}\Phi''+O(\Delta x^3), \tag{7b}$$

where the subscription of '*real*' means the physical value. Assuming Δx is sufficiently small and neglecting the higher order term of $O(\Delta x^3)$,

$$\overline{\Phi}_i<\Phi_{L,\min\,\mathrm{mod}}<\Phi_{real,i+\frac{1}{2}}<\Phi_{R,\min\,\mathrm{mod}}<\overline{\Phi}_{i+1}. \tag{8}$$

Figure 2 shows the relation between the minmod interpolation value and the physical value. Now, let us define the transferred quantity as $\Phi_{L,\frac{1}{2}}=\Phi_{R,\frac{1}{2}}=0.5(\Phi_{L,\min\,\mathrm{mod}}+\Phi_{R,\min\,\mathrm{mod}})$. Then,

$$\Phi_{L,R,\frac{1}{2}}=\Phi_{real,i+\frac{1}{2}}-\frac{\Delta x^2}{12}\Phi''+O(\Delta x^3). \tag{9}$$

Equation (9) shows that the averaged value $\Phi_{L,R,\frac{1}{2}}$ is still 2nd-order accurate. However, the error is reduced to one-fourth compared to $\Phi_{L,\min\,\mathrm{mod}}$ and is smaller than $\Phi_{L,R,\min\,\mathrm{mod}}$. Thus, the re-evaluated convective quantity, $\Phi_{L,R,\frac{1}{2}}=0.5(\Phi_{L,\min\,\mathrm{mod}}+\Phi_{R,\min\,\mathrm{mod}})$ is always closer to $\Phi_{real,i+\frac{1}{2}}$ than $\Phi_{L,\min\,\mathrm{mod}}$ and $\Phi_{R,\min\,\mathrm{mod}}$.

Next, discontinuous or rapidly varied region is examined. Discontinuous region is thoroughly different in its nature from smooth region. Variation in discontinuous region should be determined in a way that it makes the largest variation or the steepest slope possible within monotonic constraint because the derivative of $\partial\Phi_{real}/\partial x$ at discontinuity is infinite mathematically. In this case, the variation of $\left|\Phi_{L,\frac{1}{2}}-\overline{\Phi}_i\right|$ and $\left|\Phi_{R,\frac{1}{2}}-\overline{\Phi}_{i+1}\right|$ is always greater than the variation by minmod, $\left|\Phi_{L,\min\,\mathrm{mod}}-\overline{\Phi}_i\right|$ and $\left|\Phi_{R,\min\,\mathrm{mod}}-\overline{\Phi}_{i+1}\right|$ respectively.

Thus, it is expected that solution is always improved both in continuous and in discontinuous region

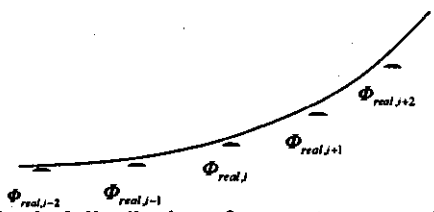

Fig. 1 Physical distribution of $\partial\Phi_{real}/\partial x>0$ and $\partial^2\Phi_{real}/\partial x^2>0$

if the convective quantity is re-evaluated as $0.5\left(\Phi_{L,\min\,mod}+\Phi_{R,\min\,mod}\right)$.

Secondly, as the most compressive second order TVD limiter, superbee limiter is considered. It chooses the steeper variation of the two candidates as

$$\phi(r)=\max\left(0,\min(2r,1),\min(r,2)\right). \tag{10}$$

From Eq.(9), we have

$$\Phi_{L,superbee}=\Phi_{real,i+\frac{1}{2}}+\frac{\Delta x^2}{6}\Phi''+O\left(\Delta x^3\right), \tag{11a}$$

$$\Phi_{R,superbee}=\Phi_{real,i+\frac{1}{2}}-\frac{\Delta x^2}{3}\Phi''+O\left(\Delta x^3\right). \tag{11b}$$

Similar to the case of minmod, we have Eq.(12) from Eq.(11)

$$\overline{\Phi}_i<\Phi_{R,superbee}<\Phi_{real,i+\frac{1}{2}}<\Phi_{L,superbee}<\overline{\Phi}_{i+1}. \tag{12}$$

Figure 3 shows the relation between superbee interpolated value and the physical value. And, the re-evaluated convective quantity is given by

$$\Phi_{L,R,\frac{1}{2}}=\Phi_{real,i+\frac{1}{2}}-\frac{\Delta x^2}{12}\Phi''+O\left(\Delta x^3\right). \tag{13}$$

Again, the error is reduced to one-fourth compared to $\Phi_{R,superbee}$ or its magnitude is smaller than that of $\Phi_{L,R,superbee}$. Thus, the re-evaluated convective quantity, $\Phi_{L,R,\frac{1}{2}}=0.5\left(\Phi_{L,superbee}+\Phi_{R,superbee}\right)$ predict a better approximation than the original interpolated values in smooth region. In discontinuous region, $\Phi_{L,superbee}$ is always larger than $\Phi_{R,superbee}$ as in Eq.(12) and thus $\left|\Phi_{L,\frac{1}{2}}-\overline{\Phi}_i\right|$ is always less than $\left|\Phi_{L,superbee}-\overline{\Phi}_i\right|$.

As a result, different from minmod limiter, accuracy is not improved with the re-evaluated quantity. It gives more numerical viscosity.

Based on the previous analysis, the case of $\partial\Phi_{real}/\partial x>0$ and $\partial^2\Phi_{real}/\partial x^2>0$ can be summarized as follows. In smooth region, the re-evaluation of $\Phi_{L,R,\frac{1}{2}}=0.5\left(\Phi_L+\Phi_R\right)$ is always expected to yield more accurate results than minmod and superbee limiters. In discontinuous region,

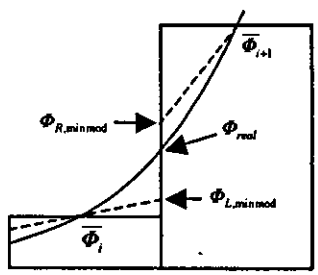

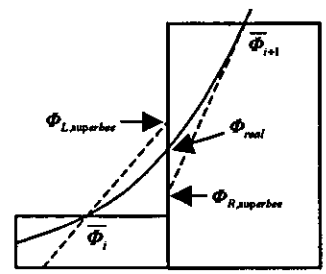

Fig. 2 Physical distribution and numerical approximation by minmod limiter (left); Fig. 3 Physical distribution and numerical approximation by superbee limiter (right)

accuracy would be enhanced only in minmod case.

Lastly, let us consider differentiable and symmetric 2nd order TVD limiters such as van Leer limiter. Then, from $\phi'(1)=0.5$ and Eq.(5b) , the leading error of the averaged value is the same as Eq.(5a). However, as will be explained in *Proposition* (Eq.(14)) and Section 3.1.2, the proposed re-evaluation always selects steeper variation and as a result numerical viscosity is reduced.

When the distribution of Φ_{real} is different, such as, $\partial\Phi_{real}/\partial x<0$ and $\partial^2\Phi_{real}/\partial x^2>0$, r_L is between 0 and 1 and r_R is between 1 and $1/r_L$. Similarly, in case of $\partial\Phi_{real}/\partial x>0$ and $\partial^2\Phi_{real}/\partial x^2<0$, $r_{L,R}$ is $0<r_L<1$ and $1<r_R<1/r_L$. In case of $\partial\Phi_{real}/\partial x<0$ and $\partial^2\Phi_{real}/\partial x^2<0$, $r_{L,R}$ is $r_L>1$ and $0<r_R<1/r_L$. Through the similar analysis, it can be shown that all other cases yield the same results.

When there is an inflection point (r_L , $r_R>1$ or $0<r_L$, $r_R<1$), the leading error of the averaged value in Eq.(5b) is the same as Eq.(5a) because of $\phi_L'(1)=\phi_R'(1)$. Lastly, overall accuracy becomes first order at local extrema. But the averaged value is still effective because the leading error term after re-evaluation is reduced by half.

Equations (8), (12) reveal an important property which should be fully exploited in evaluating limited variations. The derivative of $\partial\Phi_{real}/\partial x$ at discontinuity is infinite mathematically. Thus, when variations are estimated accordingly, the condition of $\Phi_R<\Phi_L$ (see Eq.(3)) can be readily derived as in superbee limiter, which is quite reasonable in rapidly varied region. However, if the same interpolated values are applied to gently varied region, computations is likely to be unstable due to excessive variation, or too much compression of $\Phi_{L\,or\,R}$. The computation of vortex flow in Section 4 would be a good example. The weak point of minmod and superbee limiters is due to their consistent numerical behaviors regardless of the nature of the real physical distribution.

Therefore, based on the previous analysis on TVD limiters, we identify rapidly varied region or discontinuous region by the condition of $\overline{\Phi}_i<\Phi_R<\Phi_L<\overline{\Phi}_{i+1}$. And, the criterion to distinguish gently varied region from rapidly varied region is proposed as follows.

Gently varied region: $\overline{\Phi}_i<\Phi_L<\Phi_R<\overline{\Phi}_{i+1}$ (14a)

Rapidly varied region: $\overline{\Phi}_i<\Phi_R<\Phi_L<\overline{\Phi}_{i+1}$ (14b)

Responding to the requirement *r*1 mentioned in this section, the following criterion is proposed.

(Proposition) *If the interpolated value of* $\Phi_{L\,and\,R}$ *satisfies the condition of Eq.(14a), the physical state at a cell-interface is considered to be in continuous region and the convective property at a cell-interface is modified as* $\Phi_{L,\frac{1}{2}}=\Phi_{R,\frac{1}{2}}=0.5(\Phi_L+\Phi_R)$. *If* $\Phi_{L\,and\,R}$ *satisfies the condition of Eq.(14b), it is considered to in discontinuous region and the interpolated value is not re-evaluated. Then, the re-evaluated value,* $\Phi_{L,R,\frac{1}{2}}$ *is closer to the physical value than the original interpolated value.*

Equation (14a) can be rewritten as follows.

$$\overline{\Phi}_i<\Phi_L<0.5(\Phi_L+\Phi_R)<\Phi_R<\overline{\Phi}_{i+1}. \tag{15a}$$

Or more generally,

$$\left|\Phi_L-\overline{\Phi}_i\right|\le\left|0.5(\Phi_L+\Phi_R)-\overline{\Phi}_i\right| \text{ or } (0.5(\Phi_L+\Phi_R)-\Phi_L)(\Phi_{L,superbee}-\Phi_L)\ge 0. \tag{15b}$$

Here, Φ_L lies between $\Phi_{L,\min mid}$ and $\Phi_{L,superbee}$, and the convective quantity is determined as follows.

In gently varied region, $\left(0.5(\Phi_L+\Phi_R)-\Phi_L\right)\left(\Phi_{L,superbee}-\Phi_L\right)=0.5\left(\Phi_R-\Phi_L\right)\left(\Phi_{L,superbee}-\Phi_L\right)\geq 0$,

$$\Phi_{L,i+\frac{1}{2}}=0.5\left(\Phi_L+\Phi_R\right). \tag{16a}$$

In rapidly varied region, $0.5\left(\Phi_R-\Phi_L\right)\left(\Phi_{L,superbee}-\Phi_L\right)<0$,

$$\Phi_{L,i+\frac{1}{2}}=\Phi_L. \tag{16b}$$

As a consequence, $\Phi_{L,i+\frac{1}{2}}$ always gives a larger variation, *i.e.*, less numerical dissipation than the original value and thus accuracy is enhanced.

Now, we also consider the case of general p-th order interpolation. The left and right interpolated values have the same magnitude with the opposite sign for the leading error term.

$$\Phi_L=\Phi_{real,i+\frac{1}{2}}+c\frac{\partial^p\Phi}{\partial x^p}+O\left(\Delta x^{p+1}\right), \tag{17a}$$

$$\Phi_R=\Phi_{real,i+\frac{1}{2}}-c\frac{\partial^p\Phi}{\partial x^p}+O\left(\Delta x^{p+1}\right), \tag{17b}$$

where p is an odd number.

Then, the averaged value of $\Phi_{L,\frac{1}{2}}=\Phi_{R,\frac{1}{2}}=0.5\left(\Phi_L+\Phi_R\right)$ has the $(p+1)$-th order leading error term, *i.e.*, accuracy is increased by one order of magnitude.

$$\Phi_{L,\frac{1}{2}}=\Phi_{R,\frac{1}{2}}=0.5\left(\Phi_L+\Phi_R\right)=\Phi_{real,i+\frac{1}{2}}+O\left(\Delta x^{p+1}\right). \tag{18}$$

In general, most p-th order interpolation schemes maintain the accuracy level of Eq.(17) in gently varied region. Thus, when the re-evaluated form of Eq.(18) adopts 3rd or 5th order interpolation schemes, the results in the region of $\overline{\Phi}_i<\Phi_L<\Phi_R<\overline{\Phi}_{i+1}$ is much more improved than 2nd order case.

Requirement 2:

With regard to the requirement *r*2 for the monotonic distribution, the re-evaluated value at a cell-interface should satisfy the following constraint.

$$\min\left(\Phi_{L,mn\,\mathrm{mod}},\Phi_{L,superbee}\right)\leq\Phi_{L,\frac{1}{2}}\leq\max\left(\Phi_{L,mn\,\mathrm{mod}},\Phi_{L,superbee}\right). \tag{19}$$

Many researches have been conducted to preserve accuracy at local extrema by introducing TVB[13], ENO[6], MP schemes[14], or extended TVD approaches[9, 15]. Their results show that smooth extremum can be treated successfully with less restrictive condition. For the purpose of robust convergence, however, the re-evaluation procedure adopts TVD. Equation (19) can be written as

$$\overline{\Phi}_i<\Phi_{L,\min\,\mathrm{mod}}<\Phi_{L,\frac{1}{2}}=0.5\left(\Phi_L+\Phi_R\right)<\Phi_{L,superbee}<\overline{\Phi}_{i+1}. \tag{20}$$

After applying the monotonic condition to Eq.(16), we have

$$\Phi_{L,\frac{1}{2}} = \Phi_L + sign\left(\Phi_{L,superbee} - \Phi_L\right)\min\left(\left|0.5\left(\Phi_R - \Phi_L\right)\right|, \left|\Phi_{L,superbee} - \Phi_L\right|\right). \tag{21a}$$

if $\left(\Phi_R - \Phi_L\right)\left(\Phi_{L,superbee} - \Phi_L\right) \geq 0$.

$$\Phi_{L,\frac{1}{2}} = \Phi_L, \tag{21b}$$

if $\left(\Phi_R - \Phi_L\right)\left(\Phi_{L,superbee} - \Phi_L\right) < 0$.

In brief, the property at a cell-interface can be rewritten as follows.

$$\Phi_{L,\frac{1}{2}} = \Phi_L + \frac{\max\left[0, \left(\Phi_R - \Phi_L\right)\left(\Phi_{L,superbee} - \Phi_L\right)\right]}{\left(\Phi_R - \Phi_L\right)\left|\Phi_{L,superbee} - \Phi_L\right|}\min\left[\frac{\left|\Phi_R - \Phi_L\right|}{2}, \left|\Phi_{L,superbee} - \Phi_L\right|\right], \tag{22a}$$

$$\Phi_{R,\frac{1}{2}} = \Phi_R + \frac{\max\left[0, \left(\Phi_L - \Phi_R\right)\left(\Phi_{R,superbee} - \Phi_R\right)\right]}{\left(\Phi_L - \Phi_R\right)\left|\Phi_{R,superbee} - \Phi_R\right|}\min\left[\frac{\left|\Phi_L - \Phi_R\right|}{2}, \left|\Phi_{R,superbee} - \Phi_R\right|\right]. \tag{22b}$$

Requirement 3:

Equation (22) should exhibit complete upwinding in supersonic region. However, the form of $\Phi_{1/2} = 0.5\left(\Phi_L + \Phi_R\right)$ is not correct in supersonic flows although it is appropriate in subsonic flows. This suggests that $\Phi_{1/2}$ should be determined after a cell-interface state is identified whether it belongs to subsonic or supersonic region. A simple quadratic function is introduced for that purpose, and the convective quantity at a cell-interface is finally formulated as follows.

$$\Phi_{L,\frac{1}{2}} = \Phi_L + \frac{\max\left[0, \left(\Phi_R - \Phi_L\right)\left(\Phi_{L,superbee} - \Phi_L\right)\right]}{\left(\Phi_R - \Phi_L\right)\left|\Phi_{L,superbee} - \Phi_L\right|}\min\left[a\frac{\left|\Phi_R - \Phi_L\right|}{2}, \left|\Phi_{L,superbee} - \Phi_L\right|\right], \tag{23a}$$

$$\Phi_{R,\frac{1}{2}} = \Phi_R + \frac{\max\left[0, \left(\Phi_L - \Phi_R\right)\left(\Phi_{R,superbee} - \Phi_R\right)\right]}{\left(\Phi_L - \Phi_R\right)\left|\Phi_{R,superbee} - \Phi_R\right|}\min\left[a\frac{\left|\Phi_L - \Phi_R\right|}{2}, \left|\Phi_{R,superbee} - \Phi_R\right|\right], \tag{23b}$$

where $a = 1 - \min\left(1, \max\left(\left|M_L\right|, \left|M_R\right|\right)\right)^2$, and its derivative is continuous when the Mach number becomes zero. In supersonic flows, the function a has the value of zero and

$$\Phi_{L,\frac{1}{2}} = \Phi_L, \quad \Phi_{R,\frac{1}{2}} = \Phi_R. \tag{24}$$

Although the analysis in this section is carried out using TVD limiters, the *proposition* looks general in the sense that the present approach is still available when other monotonic interpolation schemes are adopted, such as ENO and Multi-dimensional Process (MLP).

2.2. Complete monotonicity

The advection property of AUSM-type schemes may lead to undesirable overshoot problems across shock discontinuity. Figure 4 shows the typical profiles of numerical shock wave in one-point shock capturing schemes, where the *i*-th cell is intermediate. Figure 5 shows corresponding converged pressure distribution at the (*i+1*)th cell according to the intermediate Mach number of cell *i*, when the left and right physical states across the shock wave are fixed. It is found out that the converged pressure distribution of AUSM+ changes rapidly in case of $M_i^* \approx M_1^*$ or $M_i^* \approx M_2^*$, *i.e.*, when the

location of a cell-interface almost coincides with the position of shock discontinuity. In other words, pressure rapidly changes even if the Mach number changes gently. Thus, if a cell-interface is nearly aligned with physical shock wave, there is a danger that convergence becomes deteriorated. Moreover, numerical dissipation across sonic transition position disappears in a shock-aligned grid system, which also makes convergence even worse. For these reasons, it is often observed that convergence is very sensitive to grid system if $M_i^* \approx M_1^*$ or $M_i^* \approx M_2^*$.

Figure 6 is a good example showing the sensitivity of grid convergence. Depending on the location of sonic transition point with respect to a cell-interface, the behavior of computed solutions is quite different. In the initial stage of computation, numerical shock is propagated from the wall and moves toward steady shock location. During this evolution, stagnation region is continuously exposed to numerical error generated by numerical shock wave, and contaminated stagnation region changes shock location again. In this situation, if pressure changes rapidly according to the Mach number at the intermediate cell, it is very difficult to obtain a converged solution. At the worst case, a converged solution can not be obtained at all like Fig. 6(a). In order to prevent this phenomenon completely, the interaction between shock discontinuity and stagnation region due to numerical error should be eliminated. Figure 6(c) shows the converged result by AUSM+, which is obtained from the converged result of Fig. 6(b) by M-AUSMPW+.

The pressure splitting function is modified to reduce grid dependency and improve convergence characteristics in steady shock discontinuity. Most useful relations in realizing a numerical shock profile are the Rankine-Hugoniot or the Prandtl relation. Roe's FDS exploits the Rankine-Hugoniot relation and AUSM-type schemes use the Prandtl relation. Unlike the Rankine-Hugoniot relation which includes the relation among thermodynamic variables such as density, pressure and temperature, the Prandtl relation does not possess the information. This lack of information does lead to non-monotonic overshoots or slightly diffusive results of a discrete shock profile. In M-AUSMPW+, this defect is cured by the information on pressure jump across a shock, directly derived from the governing equations.

Let us consider a one-dimensional stationary shock wave with $c_s = c^*$. Then, from the Prandtl relation, $M_1^* M_2^* = 1$. It is assumed that shock is captured with only one intermediate cell and sonic

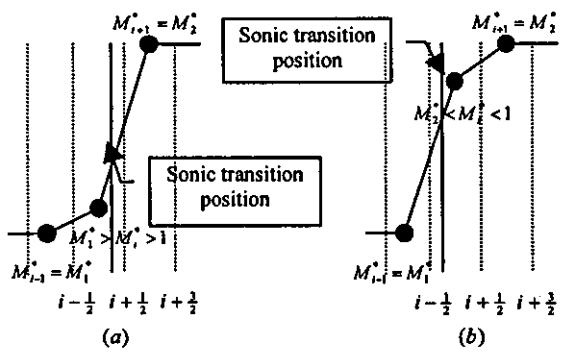

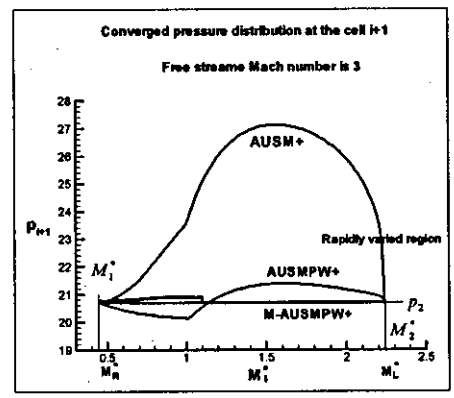

Fig. 4 Numerical shock profile of one point shock capturing scheme (left); Fig. 5 Comparison of pressure overshoots according to the Mach number at an intermediate cell (right)

transition position is located between i-th cell and the cell-interface $i+\frac{1}{2}$, as in Fig.4(a). Then,

$$F_{i+\frac{1}{2}} = F_{i+\frac{3}{2}} = u_2 \Psi_2 + \mathbf{P}_2 . \tag{25}$$

Here, $u_2\Psi_2 + \mathbf{P}_2$ denotes the physical flux after shock wave. Thus,

$$U_i \Psi_i + M_{i+1}^{-} c_{i+\frac{1}{2}} \Psi_{i+1} + \mathbf{P}_i + \mathbf{P}_{i+1} P_{i+1}^{-} = U_{i+1} \Psi_{i+1} + \mathbf{P}_{i+1} = U_2 \Psi_2 + \mathbf{P}_2 , \tag{26a}$$

$$U_i \Psi_i + \mathbf{P}_i = M_{i+1}^{+} c_{i+\frac{1}{2}} \Psi_{i+1} + \mathbf{P}_{i+1} P_{i+1}^{+} . \tag{26b}$$

Continuity equation: $$\rho_i U_i = \rho_{i+1} M_{i+1}^{+} c_{i+\frac{1}{2}} . \tag{27a}$$

Momentum equation: $$\rho_i U_i U_i + p_i = \rho_{i+1} M_{i+1}^{+} c_{i+\frac{1}{2}} U_{i+1} + \left(1 - P_{i+1}^{-}\right) p_{i+1} . \tag{27b}$$

Energy equation: $$\rho_i U_i H_i = \rho_{i+1} M_{i+1}^{+} c_{i+\frac{1}{2}} H_{i+1} \tag{27c}$$

Since the total enthalpy should be constant in a steady flow, energy equation is always satisfied only if continuity equation is satisfied. From Eqs.(27a) and (27b), the information on pressure jump across a shock can be obtained as follows.

$$\rho_i U_i U_i + p_i = \rho_i U_i U_{i+1} + \left(1 - P_{i+1}^{-}\right) p_{i+1} , \tag{28a}$$

$$P_{i+1}^{-} = 1 - \frac{\rho_i U_i \left(U_i - U_{i+1}\right) + p_i}{p_{i+1}} . \tag{28b}$$

Equation (28) compensates the missing information among thermodynamic variables across shock. In case of Fig.4(b), pressure splitting function does not need to be modified since shock turns out to be stable and maintains a monotonic profile [12]. Thus, the modified form of pressure splitting function is written as follows.

If $M_i^{*} > 1$, $M_{i+1}^{*} < 1$ and $0 < M_i^{*} M_{i+1}^{*} < 1$,

$$P_{i+1}^{-} = 1 - \frac{\rho_i U_i \left(U_i - U_{i+1}\right) + p_i}{p_{i+1}} . \tag{29a}$$

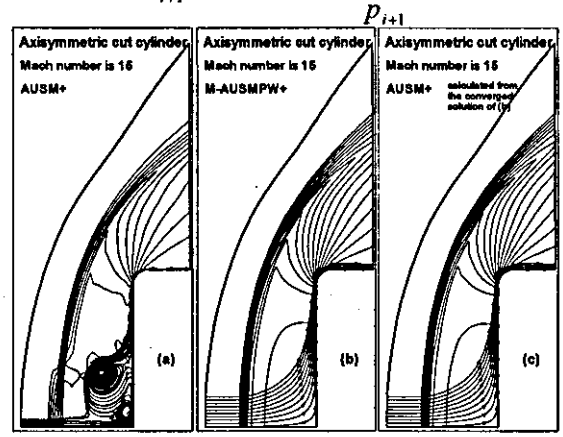

Fig. 6 Pressure contours and streamlines around a cut cylinder

If $M_i^* > -1$, $M_{i+1}^* < -1$ and $0 < M_i^* M_{i+1}^* < 1$,

$$P_i^+ = 1 - \frac{\rho_{i+1} U_{i+1}(U_{i+1} - U_i) + p_{i+1}}{p_i}. \tag{29b}$$

Otherwise, it keeps the original form.

If computation reaches a steady state, Eq.(29) is distributed as in Fig.7 showing that the positivity of the modified pressure splitting function. In transient process to obtain a steady state solution, however, the positivity of Eq.(29) may not be guaranteed due to numerical error. Thus, the following form is adopted just for stable computation

If $M_i^* > 1$, $M_{i+1}^* < 1$ and $0 < M_i^* M_{i+1}^* < 1$,

$$P_{i+1}^- = \max\left(0, \min\left(0.5, 1 - \frac{\rho_i U_i (U_i - U_{i+1}) + p_i}{p_{i+1}}\right)\right). \tag{30a}$$

If $M_i^* > -1$, $M_{i+1}^* < -1$ and $0 < M_i^* M_{i+1}^* < 1$,

$$P_i^+ = \max\left(0, \min\left(0.5, 1 - \frac{\rho_{i+1} U_{i+1} (U_{i+1} - U_i) + p_{i+1}}{p_i}\right)\right). \tag{30b}$$

Figures 5 and 6(b) clearly shows the effect of the modified pressure splitting function.

The modification of the pressure splitting function can be examined in several flow conditions. Let us consider the four different cases at a cell-interface across sonic transition position: compression shock wave, expansion shock wave, continuous compression flow, and continuous expansion flow.

In case of expansion flows, the modification is not turned on. Since the derivative of the original pressure splitting function is continuous, a continuous solution can be obtained. Especially, the present scheme does not admit expansion shock condition by the proper action of numerical dissipation [1].

In case of compression shock, the derivative of the modified pressure splitting function is discontinuous across sonic transition position. The derivative does not have to be continuous in numerical shock region. Numerical shock wave is always captured with some intermediate states.

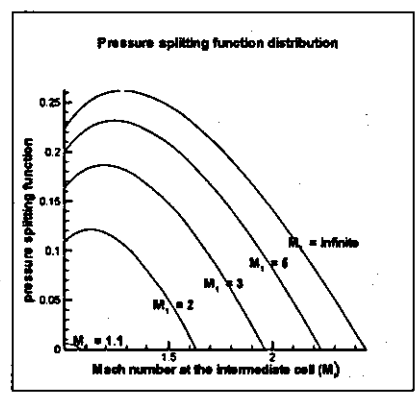

Fig. 7 Plot of pressure splitting function (Eq.(29)) according to the Mach number at an intermediate cell

Contrary to flow physics, numerical mass flux at the intermediate cell cannot be conversed. Thus, the property at the intermediate cell can be treated as purely numerical values, *i.e.*, there is no physical meaning. If the pressure splitting function is modified, it just means that the property at the intermediate cell is determined just for the purpose of numerical stability. In this respect, the modification never makes a problem even if its first derivative is not continuous. Lastly, in case of continuous compression wave, the non-smoothness may generate some problem.

In actual computations, it does not cause any problem especially when a higher order spatial accuracy is used. Since left and the right values are very close to each other, $p_L \approx p_R$ and $M_{L,R} \approx 1$ and $P_R^- \to 0$ or $M_{L,R} \approx -1$ and $P_L^+ \to 0$. As a consequence, the modification is useful for a steady flow calculation and grid dependency is considerably reduced.

Even though the modification is derived under steady flow assumption, it can be used optionally for unsteady cases. It works successfully in unsteady shock wave without any numerical instability, which is verified with moving shock wave .

Summarizing the previous analyses, the M-AUSMPW+ can be written as follows.

$$\mathbf{F}_{\frac{1}{2}} = \overline{M}_L^+ c_{\frac{1}{2}} \Psi_{L,\frac{1}{2}} + \overline{M}_R^- c_{\frac{1}{2}} \Psi_{R,\frac{1}{2}} + \left(\mathrm{P}_L^+ \mathbf{P}_L + \mathrm{P}_R^- \mathbf{P}_R\right), \tag{31a}$$

where $P_{L,R} = \left(0, n_x p_{L,R}, n_y p_{L,R}, 0\right)^T$ and $n_{x,y}$ are the components of (x,y) normal vector of a cell-interface.

The convective vector, Ψ are

$$\Psi_{L,R,\frac{1}{2}} = \begin{pmatrix} \rho_{L,R,\frac{1}{2}} \\ \rho_{L,R,\frac{1}{2}} u_{L,R,\frac{1}{2}} \\ \rho_{L,R,\frac{1}{2}} v_{L,R,\frac{1}{2}} \\ \rho_{L,R,\frac{1}{2}} H_{L,R,\frac{1}{2}} \end{pmatrix}, \tag{31b}$$

where $H_{L,R,\frac{1}{2}} = \dfrac{\gamma}{\gamma - 1} \dfrac{p_{L,R,\frac{1}{2}}}{\rho_{L,R,\frac{1}{2}}} + 0.5\left(u^2_{L,R,\frac{1}{2}} + v^2_{L,R,\frac{1}{2}}\right)$.

Re-evaluated quantities at a cell-interface are obtained from Eq.(23). $\overline{M}^{\pm}_{L,R}$, $P^{\pm}_{L,R}$ and the speed of sound at a cell-interface are the same as in AUSMPW+.

3. Numerical Result

3.1. Stationary vortex flow

Vortex flow is characterized by the existence of negative pressure gradient toward core and curved streamlines. Thus, it can be regarded as a pure multi-dimensional phenomenon, and in most applications, it is very difficult or impossible that the flow is aligned with grid system. Moreover, in core region where pressure gradient changes very steeply, computed results are smeared very much.

Vortex model is Thomson-Rankine vortex model which is composed of free vortex outside the core and forced vortex inside the core.

a. free vortex (outside the core): $V_\theta \cdot r = const$ and $\frac{1}{\rho}\frac{\partial p}{\partial r} = \frac{V_\theta^2}{r}$. (32a)

b. forced vortex (inside the core): $V_\theta = \omega \cdot r$ and $\frac{dp}{dr} = \rho\frac{V_\theta^2}{r}$. (32b)

Angular velocity ω is 3, core radius is 0.2 and maximum velocity is $0.54c_\infty$. Total computational domain is from -2 to 2 with equal spacing. For grid convergence test, 25 by 25, 50 by 50, 75 by 75 and 100 by 100 grid points are selected. Roe's FDS, AUSMPW+ and M-AUSMPW+ are used for numerical fluxes. 3rd order TVD Runge-Kutta time integration is used and CFL number is 0.8. Boundary conditions are fixed as initial values. Pressure distribution is plotted at the non-dimensionalized time of 40. Figure 8 shows density distributions according to numerical fluxes, plotted along the line AB. Figure 8(a) is the result of minmod limiter. Roe's FDS and AUSMPW+ results are somewhat diffusive but M-AUSMPW+ provides much more improved result. Compared to the result by AUSMPW+ on four times denser grid system, M-AUSMPW+ is about twice more accurate. A similar tendency in accuracy improvement can be observed when van Leer limiter is used.

Figure 9 is the comparison of entropy variation and Fig. 10 is the characteristics of grid convergence. As expected, entropy increase is minimal in case of M-AUSMPW+. M-AUSMPW+ with van Leer limiter is asymptotically close to the result by AUSMPW+ with 3rd order interpolation without any limiting function. The result of superbee limiter is not included, because vortex strength is artificially amplified as computation continues, *i.e.*, entropy is decreasing continuously and finally computation fails. Thus, superbee limiter cannot be used for this type of flows, even though it gives the best results in a contact or a slip discontinuity. Aside from the reason, it has monotonicity and convergence problems in multi-dimensional flows. In this respect, M-AUSMPW+ can be one of the best choices for multi-dimensional flows without compromising the accuracy in a contact or slip discontinuity.

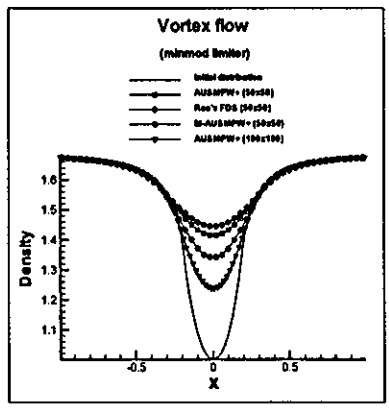

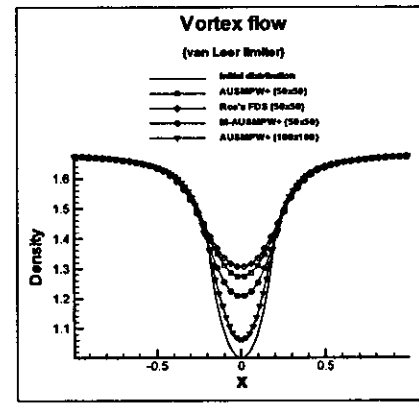

Fig. 8(a) Comparison of density distribution along the line AB (minmod limiter) (left); Fig. 8(b) Comparison of density distribution along the line AB (van Leer limiter) (right)

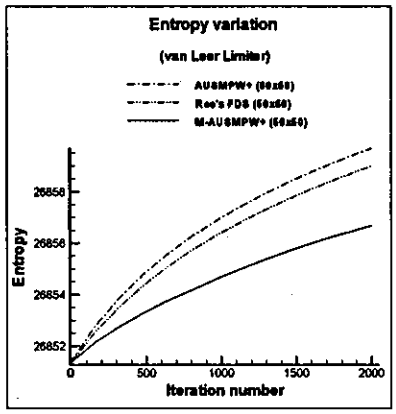

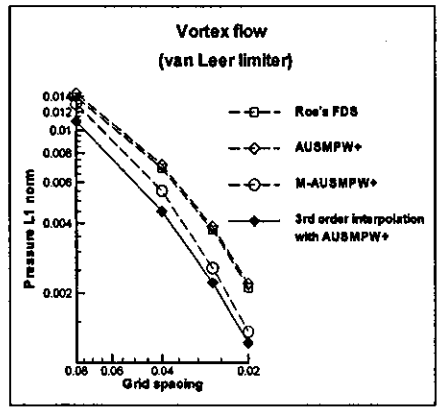

Fig. 9 Comparison of entropy variation (van Leer limiter) (left); Fig. 10 comparison of grid convergence test according to flux functions (van Leer limiter) (right)

3.2. Viscous Shock tube problem

This test problem was studied by Daru and Tenaud [16] and Sjögreen and Yee [17]. It is a shock tube problem in 2-D square box with unit length, $0 \le x, y < 1$, and the diaphragm is located at $x = 0.5$. The initial state is given as follows.

$$(\rho, u, v, p)_L = (120,0,0,120/\gamma) \text{ and } (\rho, u, v, p)_R = (1.2,0,0,1.2/\gamma).$$

The Reynolds number is 200 and the viscosity is constant. For the fair comparison of AUSMPW+ and M-AUSMPW+, the viscous flux terms of the governing equations are calculated by 4th order interpolation.

At $t = 0$, diaphragm is broken and the shock wave moves toward $x = 1$. Then, it is reflected and complex flow interactions occur. 3rd order TVD Runge-Kutta time integration is used and the results are at non-dimensionalized time of 1. CFL number is 0.5. Figure 11(a) is the comparison of the density

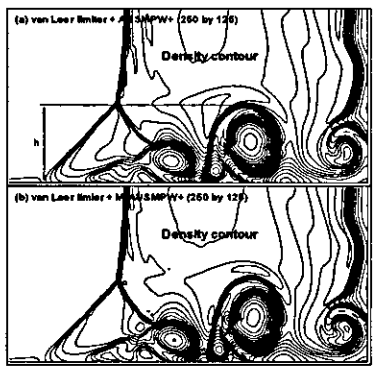

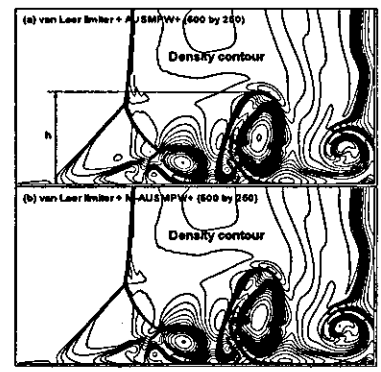

Fig. 11(a) Comparison of density distribution of AUSMPW+ and M-AUSMPW+ (250 by 125) (left); Fig. 11(b) Comparison of density distribution of AUSMPW+ and M-AUSMPW+ (500 by 250) (right)

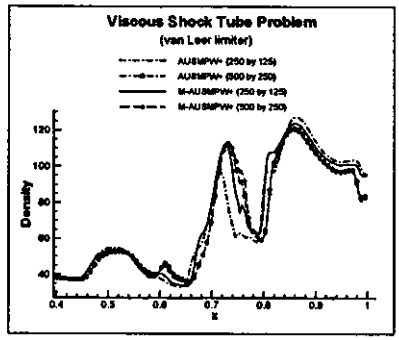

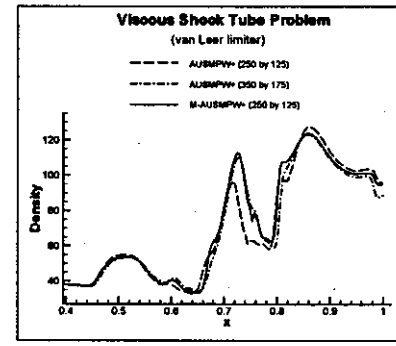

Fig. 12(a) Comparison of density distribution along the wall (left); Fig. 12(b) Comparison of density distribution along the wall (right)

Table 1. Comparison of the height of primary vortex

Scheme	AUSMPW+ (van Leer limiter) (250 by 125)	M-AUSMPW+ (van Leer limiter) (250 by 125)	AUSMPW+ (van Leer limiter) (350 by 175)	AUSMPW+ (van Leer limiter) (500 by 250)	M-AUSMPW+ (van Leer limiter) (500 by 250)
Height (h)	0.142	0.154	0.155	0.163	0.166

contour of AUSMPW+ and M-AUSMPW+ with van Leer limiter. The grid size is 250 by 125. Figure 11(b) is the results on 500 by 250 grid system.

After the interaction between boundary layer and the lambda shock, vortices due to flow separation are generated and they grow up on the downstream side. From Ref.[17], the results with 500 by 250 grid system is very similar to the grid converged solution. Due to the effect of numerical dissipation in multi-dimensional flows, the growth of the primary vortex by AUSMPW+ in Fig.11(a) is relatively slower and it is less rotated compared with the results of M-AUSMPW+. Figure 12(a) shows that more clearly. The nearest solution to the grid converged solution is the result of M-AUSMPW+ on 500 by 250 grid system. AUSMPW+ is certainly much more diffusive than M-AUSMPW+ on 250 by 125 grid system. Figure 12(b) shows that the result of M-AUSMPW+ by 250 x 125 (=31250) grids is almost the same with AUSMPW+ by 350 x 175 (=61250) grids. Table 1 is the comparison of primary vortex size. It is confirmed again that M-AUSMPW+ can provides the same accuracy with half grid points.

From the numerous test cases and analyses, M-AUSMPW+ is shown to provide the accuracy enhancement in continuous region as well as in discontinuous region, especially, in multi-dimensional flow situations. By implementing M-AUSMPW+ in three-dimensional computations, the accuracy improvement is expected to be more visible: M-AUSMPW+ can present the grid reduction effect to $2^{-3/2}$ in three-dimensional computations.

3.3. Shock wave / boundary-layer interaction

The shock wave/boundary-layer interaction problem has been widely used for a viscous flow validation. The free stream Mach number is 2 and the shock impinging angle is 32.5 degree. Reynolds

number is 2.96×10^5. The grid system is 56 by 59 and the denser grid is 150 by 200. It is known as a steady problem and AF-ADI is used for temporal integration. Figure 13 shows the comparison of pressure contours between Roe's FDS and M-AUSMPW+ with van Leer limiter. Figure 14 is the pressure distribution along the line AB. The flow structure by M-AUSMPW+ presents expansion and re-compression waves more clearly because separated flow is resolved more accurately. Figure 15 shows the comparison of skin friction coefficients. Since separated flow is not aligned with grid lines, a scheme should capture oblique contact discontinuity accurately for the accurate calculation of separation region. M-AUSMPW+ is expected to improve accuracy significantly in this region. It is certified by Figs. 15(a) and 15(b). Separation region by M-AUSMPW+ is closer to the result on denser grid system. Figure 15(c) and Table 2 show the comparison of area ratio in separation region. Separation region by Roe's FDS with minmod limiter is very narrow but the same computation by M-AUSMPW+ is similar to Roe's FDS with van Leer limiter. Also, M-AUSMPW+ with van Leer limiter shows a significant accuracy enhancement and separation region is very close to the result on denser grid system. Figure 16 shows the error history of M-AUSMPW+. Convergence characteristic is similar to Roe's FDS or AUSMPW+.

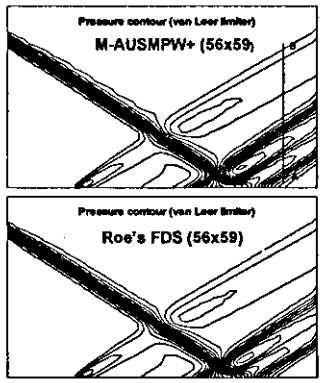

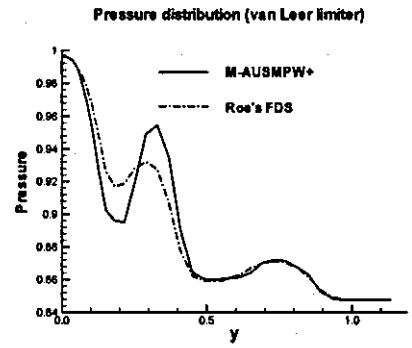

Fig. 13 Comparison of pressure contours (van Leer Limiter) (left); Fig. 14 Comparison of pressure distribution along the line AB (van Leer Limiter) (right)

Table 2. Comparison of the area ratio of separation region

Scheme	Roe's FDS (van Leer limiter) (150 by 200)	M-AUSMPW+ (van Leer limiter) (56 by 59)	M-AUSMPW+ (minmod limiter) (56 by 59)	Roe's FDS (van Leer limiter) (56 by 59)	Roe's FDS (minmod limiter) (56 by 59)
Area ratio+	1	0.912	0.539	0.600	0.220

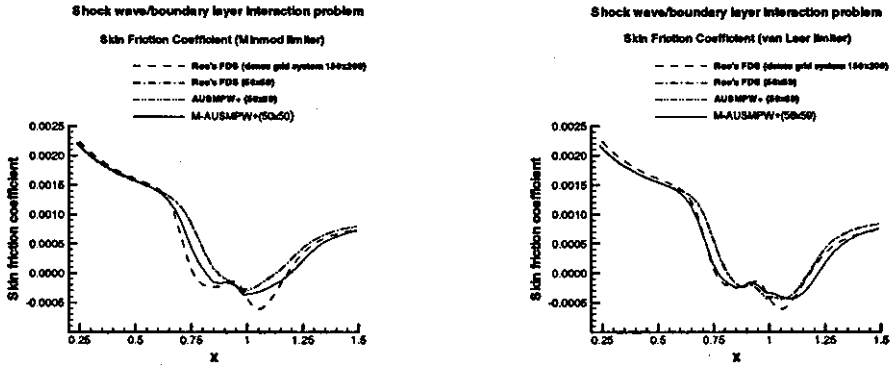

Fig. 15(a) Comparison of skin friction coefficient (minmod Limiter) (left); Fig. 15(b) Comparison of skin friction coefficient (van Leer Limiter) (right)

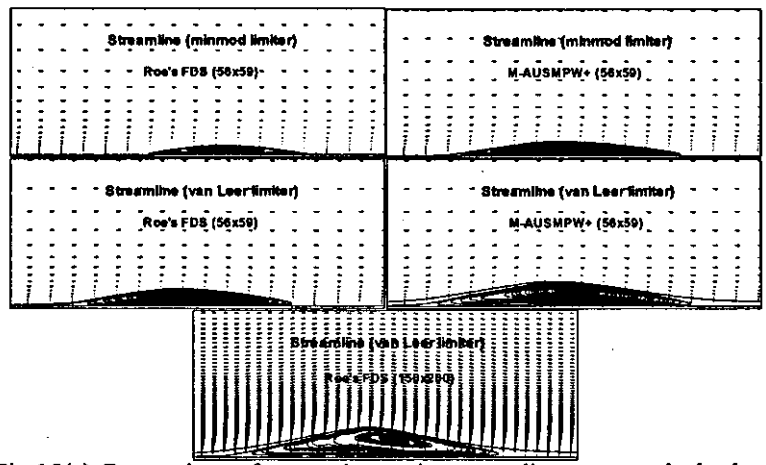

Fig.15(c) Comparison of separation region according to numerical schemes

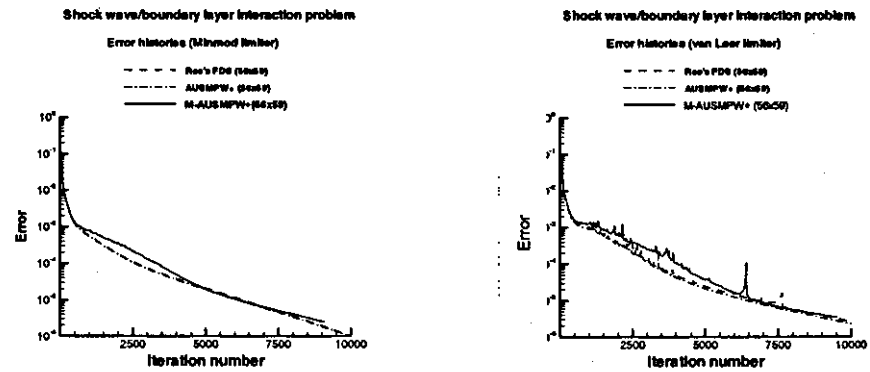

Fig. 16(a) Comparison of convergence (minmod Limiter) (left); Fig. 16(b) Comparison of convergence (van Leer Limiter) (right)

4. CONCLUSIONS

A new treatment of a cell-interface convective flux which typically appears in AUSM-type methods is introduced to substantially reduce numerical dissipation in smooth region without compromising accuracy in shock region. The core idea of the new method is to modify the convective quantity at a cell-interface by considering flow physics. Through the analysis of TVD limiters, a simple criterion to predict a more accurate cell-interface state is proposed and the convective quantity is re-evaluated according to the criterion. The practical advantages of the proposed method can be revealed in two aspects. One is that the newly defined cell-interface value is closer to the real physical value. The other is that it can eliminate numerical dissipation effectively in non-flow aligned grid system. Thus, M-AUSMPW+, a new scheme formulated by incorporating the re-evaluation procedure, improves solution accuracy significantly in multi-dimensional problems.

Another desirable characteristic of M-AUSMPW+ is monotonicity in capturing a steady shock wave, regardless of the location of sonic transition position. As a result, convergence characteristics and grid dependency of AUSM-type methods are remarkably enhanced.

Through numerous test cases such as stationary and moving physical discontinuities, rarefaction wave, vortex flow, shock wave/boundary-layer interaction, and viscous shock tube problem, M-AUSMPW+ is proved to be equally efficient but about twice more accurate than previous schemes. If M-AUSMPW+ would be applied to three-dimensional problems, accuracy and efficiency is expected to be improved further.

ACKNOWLEDGEMENT

The authors appreciate financial support by the Korea Science and Engineering Foundation (Grant R01-2005-000-10059-0) and Agency for Defense Development and by FVRC (Flight Vehicle Research Center), Seoul National University.

REFERENCES

[1] K. H. Kim, C. Kim and O. H. Rho, Methods for the Accurate Computations of Hypersonic Flows, Part I: AUSMPW+ Scheme, *J. of Computational Physics* **174**(2001), 38-80.

[2] M. S. Liou, A Sequel to AUSM: AUSM+, *J. of Computational Physics*, **129**(1996), 364-382.

[3] A. Harten, High Resolution Schemes for Hyperbolic Conservation Laws, *J. of Computational Physics*, **49**(3)(1983), 357-393.

[4] P. K. Sweby, High Resolution Schemes Using Flux Limiters for Hyperbolic Conservation Laws, *SIAM Journal on Numerical Analysis*, **21**(5)(1984), 995-1011.

[5] C. Hirsh, Numerical Computation of Internal and External Flows, Vol. 1,2, (John Wiley & Sons, 1990).

[6] A. Harten, B. Enquist, S. Osher, and S. R. Chakravarthy, Uniformly High Order Accurate Essentially Non-oscillatory Schemes III, *J. of Computational Physics*, **71**(2)(1987), 231-303.

[7] A. Harten and S. Osher, Uniformly high order accurate non-oscillatory schemes I, *SIAM Journal on Numertical Analysis*, **24**(1987), 279-309.

[8] C. W. Shu and S. Osher, Efficient Implementation of Essentially Non-oscillatory Shock-capturing Schemes, *J. of Computational Physics*, 77(1988), 439-471.

[9] D. Pan and S. C. Lee, A fixed-stencil non-oscillatory scheme for hyperbolic systems, *J. of*

Computational Physics, **100**(1992), 200-204.
[10] X-D. Liu, S. Osher, and T. Chan, Weighted Essentially Non-Oscillatory Schemes, *J. of Computational Physics*, **115**(1994), 200-212.
[11] G. S. Jiang and C. W. Shu, Efficient Implementation of Weighted ENO Schemes, *J. of Computational Physics*, **126**(1996), 202-228.
[12] K. H. Kim, C. Kim and O. H. Rho, A Study on the Monotonic Characteristic of AUSM-type Schemes in Shock Regions, *ICAS*, Toronto, September, 2002.
[13] C. W. Shu, TVB Uniformly High-Order Schemes for Conservation Laws, *Mathematics of Computation*, **49**(179)(1987), 105-121.
[14] A. Suresh and H. T. Huynh, Accurate Monotonicity-Preserving Schemes with Runge–Kutta Time Stepping, *J. of Computational Physics*, **136**(1997), 83–99
[15] G. Billet and O. Louedin, Adaptive Limiters for Improving the Accuracy of the MUSCL Approach for Unsteady Flows, *J. of Computational Physics*, **170**(2001), 161-183.
[16] V. Daru, C. Tenaud, Evaluation of TVD high resolution schemes for unsteady viscous shocked flows, *Computers and Fluids*, **30**(2001), 89-113.
[17] B. Sjögreen, H. C. Yee, Grid convergence of high order methods for multiscale complex unsteady viscous compressible flows, *J. of Computational Physics*, **185**(2003), 1-26.

Kyung-Lok Lee
2004 B.S. Mechanical and Aerospace Engineering, Seoul National University

Sung-Hwan Yoon
2003 B.S. Mechanical and Aerospace Engineering, Seoul National University
2005 M.S. Mechanical and Aerospace Engineering, Seoul National University

Chongam Kim
E-mail : chongam@snu.ac.kr
1988 B.S. Aerospace Engineering, Seoul National University
1990 M.S. Aerospace Engineering, Seoul National University
1997 Ph.D Mechanical and Aerospace Engineering, Princeton University
1997~1998 Stanford University Center for Turbulence Research / Research Fellow
1998~1999 Instructor, Dept. of Mechanical and Aerospace Engineering, Seoul National University
2000~2004 Assistant Professor, Dept. of Mechanical and Aerospace Engineering, Seoul National University
2004~present Associate Professor, Dept. of Mechanical and Aerospace Engineering, Seoul National University
Research Field : Numerical method for computational physics
Application of gaskinetic schemes in CFD
Hypersonic and high temperature gas dynamics
Aerodynamic shape optimization and flow control
Unstructured based flow solver and mesh generation

Kyu-Hong Kim
E-mail : aerocfd1@snu.ac.kr
1994 B.S. Aerospace Engineering, Seoul National University
1997 M.S. Aerospace Engineering, Seoul National University
2001 Ph.D Mechanical and Aerospace Engineering, Seoul National University
2004~present Assistant Professor, Dept. of Mechanical and Aerospace Engineering, Seoul National University
Research Field : Numerical algorithm development for non-equilibrium hypersonic flows
Reentry aerodynamics including non-equilibrium reactive gas, rarified gas, radiation
High temperature magneto-hydrodynamics